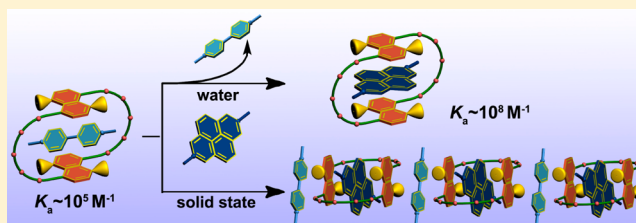


# Thermodynamics and Structures of Complexation between Tetrasulfonated 1,5-Dinaphtho-38-crown-10 and Diquaternary Salts in Aqueous Solution

Ying-Ming Zhang,<sup>†</sup> Ze Wang,<sup>†</sup> Ling Chen,<sup>†,‡</sup> Hai-Bin Song,<sup>†</sup> and Yu Liu<sup>\*,†</sup><sup>†</sup>Department of Chemistry, State Key Laboratory of Elemento-Organic Chemistry, Nankai University, Collaborative Innovation Center of Chemical Science and Engineering, Tianjin 300071, People's Republic of China<sup>‡</sup>College of Chemistry and Chemical Engineering, Jiangxi Normal University, Nanchang, Jiangxi 330022, People's Republic of China

## Supporting Information

**ABSTRACT:** The readily available recognition motifs with high affinity and selectivity can undoubtedly expedite the development of host–guest chemistry from fundamental research to practical application in miscellaneous fields. In this work, a series of guest-mediated [2]pseudorotaxanes are successfully constructed by the incorporation of tetrasulfonated 1,5-dinaphtho-38-crown-10 ( $1^{4-}$ ) with three kinds of dicationic substrates, i.e., the diquaternary salts of 4,4'-bipyridine, 1,10-phenanthroline, and 2,7-diazapyrene, which are comprehensively explored by means of UV/vis,  $^1\text{H}$  NMR spectra, X-ray crystallography, and microcalorimetric titrations. Significantly, the interpenetration of  $1^{4-}$  with  $N,N'$ -dimethyl-2,7-diazapyrenium salt (DMDAP $^{2+}$ ) gives an extraordinarily strong association constant ( $K_a$ ) up to  $10^8 \text{ M}^{-1}$  order of magnitude in water. Moreover, the spectroscopic and crystallographic analyses jointly demonstrate that there is a competitive binding process in the complexation of  $1^{4-}$  with DMDAP $^{2+}$  and methyl viologen ( $\text{MV}^{2+}$ ), in which DMDAP $^{2+}$  is internally encapsulated in the cavity of  $1^{4-}$ , whereas  $\text{MV}^{2+}$  is externally embedded in the crystallographic lattice to form the ternary supramolecular assembly of  $\text{MV}^{2+}\cdot\text{DMDAP}^{2+}\cdot\text{C}1^{4-}$ . We also envision that the  $K_a$  gradient obtained in our systematic work illustrates a new and elegant strategy for attaining multicomponent nanomaterials engineered at a molecular level.



## INTRODUCTION

The pursuit of perfection in selectivity–affinity correlations is considered as one of the fundamental and significant topics in supramolecular chemistry.<sup>1–7</sup> Among the most commonly employed components, the macrocyclic synthetic receptors, such as crown ether,<sup>8–10</sup> cyclodextrin,<sup>11–14</sup> calixarene,<sup>15–17</sup> and cucurbituril,<sup>18–21</sup> are believed to be superior candidates in the fabrication of highly ordered supramolecular architectures. However, as compared with other classic supramolecular couples with high associate constants ( $K_a$ ) and multidimensional nanoarchitectures in water, i.e., native  $\beta$ -cyclodextrin/adamantane ( $K_a$  up to  $10^4 \text{ M}^{-1}$ ),<sup>22</sup> permethyl  $\beta$ -cyclodextrin/porphyrin ( $K_a$  up to  $10^8 \text{ M}^{-1}$ ),<sup>23</sup> and cucurbit[7]uril/ferrocene ( $K_a$  up to  $10^{12} \text{ M}^{-1}$ ),<sup>24,25</sup> the diversity and complexity in the host–guest recognition involving water-soluble crown ethers have not been well established yet, probably due to the assumption that water molecules may cause serious interference with the ion–dipole interaction between the polyether chains of crown ethers and cationic substrates in aqueous media.<sup>26</sup>

Recently, considerable endeavor has been devoted to the development of water-soluble crown ethers by our group<sup>27–29</sup> and other investigators.<sup>30–33</sup> Of which, as a negatively charged receptor, the tetrasulfonato crown ether with electron-rich cavity represents a powerful host for the complexation with

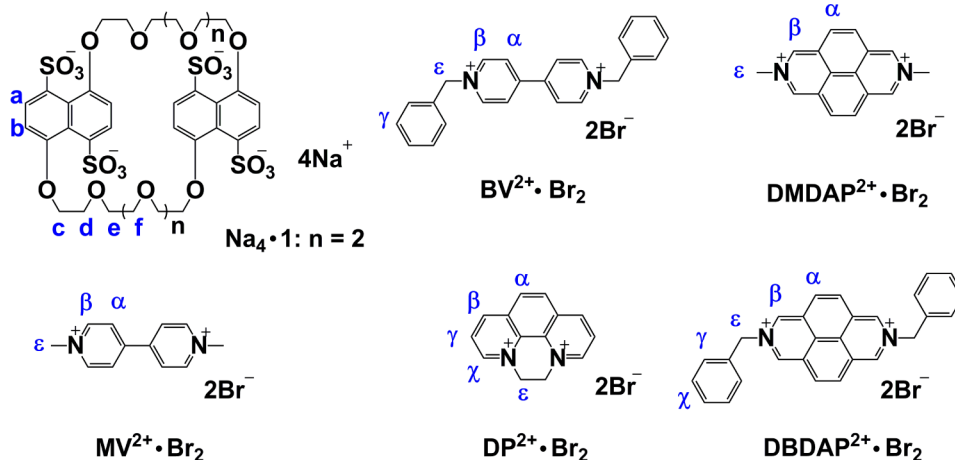
various organic cations in water. For instance, among our representative water-soluble crown ethers, it is found that the  $K_a$  values of tetrasulfonated 1,5-dinaphtho-38-crown-10 ( $1^{4-}$ ) with methyl viologen ( $\text{MV}^{2+}$ ) and the dicationic naphthalene diimide derivative (NDI $^{2+}$ ) were obtained as  $3.25 \times 10^5$  and  $2.33 \times 10^6 \text{ M}^{-1}$ , respectively.<sup>28,29</sup> In this case, the guest selectivity was somewhat lower ( $K_a^{\text{NDI}^{2+}\cdot\text{C}1^{4-}}/K_a^{\text{MV}^{2+}\cdot\text{C}1^{4-}} = 7.17$ ), mainly because the non-pyridinium salts could only eliminate the intramolecular electrostatic repulsion in the negatively charged host to a certain extent. Under such circumstance, it has been preliminarily revealed that the electrostatic attraction, as compared to the  $\pi$ -stacking interaction, is more prominent in the formation of electrically interpenetrated complexes. Nevertheless, these findings prompt us to hypothesize that an enhanced binding affinity may be achieved in  $1^{4-}$  through the incorporation with some appropriate guests possessing larger  $\pi$ -aromatic cores, because a significant  $\pi$ -stacking interaction originating from the greater size-fit efficiency will maintain and even expand its superiority in governing the molecular recognition process.

Received: November 8, 2013

Revised: January 20, 2014

Published: February 17, 2014

Chart 1. Structures and Proton Designations of Host and Guest Molecules



To test this hypothesis, in the present work, two of the most frequently encountered 2,7-diazapyrenium dications ( $\text{DAP}^{2+}$ )<sup>34–38</sup> with comparable molecular size to  $\text{NDI}^{2+}$ ,  $N,N'$ -dimethyl-2,7-diazapyrenium ( $\text{DMDAP}^{2+}$ ) and  $N,N'$ -dibenzyl-2,7-diazapyrenium ( $\text{DBDAP}^{2+}$ ), were chosen to systematically study the cooperative  $\pi$ -stacking interactions in  $1^{4-}$ , with the final goal to enhance the binding ability of flexible and nonpreorganized macrocyclic compounds. Furthermore, in order to demonstrate the roles of  $\pi$ -conjugate and substituent effect clearly, the diquaternary salts of 4,4'-bipyridine ( $\text{BV}^{2+}$ ) and 1,10-phenanthroline ( $\text{DP}^{2+}$ ) were also synthesized as the reference compounds. The molecular structures of tetrasulfonated crown ether  $1^{4-}$  and the corresponding dicationic guests are depicted in Chart 1.

As expected, benefitting from the favorable  $\pi$ -stacking arrangement, the  $K_a$  value of complex  $\text{DMDAP}^{2+}\text{C}1^{4-}$  in this research can reach up to  $10^8 \text{ M}^{-1}$  order of magnitude with an extremely higher guest selectivity ( $K_a^{\text{DMDAP}^{2+}\text{C}1^{4-}}/K_a^{\text{MV}^{2+}\text{C}1^{4-}} = 345$ ), suggesting that the  $\pi$ -stacking interaction is the main driving force in the host–guest complexation process with the larger and planar  $\pi$ -aromatic guests. More significantly, utilizing the directionally ordered  $\pi$ -stacking interaction and the binding differences between the interior cavity and exterior surface of water-soluble crown ether, we successfully constructed a ternary self-assembly of  $\text{MV}^{2+}\cdot\text{DMDAP}^{2+}\text{C}1^{4-}$  in both aqueous solution and the solid state. Our obtained results will energize the potential use of water-soluble crown ethers in the construction of functionalized supramolecular materials.

## RESULTS AND DISCUSSION

### UV/Vis Spectroscopy and Electrochemical Properties.

First of all, the charge transfer (CT) interaction arising from the  $\pi$ - $\pi$  stacking between the electron-rich donors and electron-deficient acceptors was preliminarily investigated by the method of UV/vis spectroscopy in water.<sup>39</sup> In comparison to the spectral sum of individual components, the equimolar mixing of the aqueous solutions containing  $1^{4-}$  and those aromatic substrates can induce a noticeable change in the long-wavelength region. As discerned from Figure 1a and Supporting Information (SI) Figure S4a, there was no absorption beyond 430 nm for  $1^{4-}$ ,  $\text{DMDAP}^{2+}$ , or  $\text{DBDAP}^{2+}$ , whereas the appearance of a broad band ranging from 440 to 500 nm was observed in the complexes of  $\text{DMDAP}^{2+}\text{C}1^{4-}$  and  $\text{DBDAP}^{2+}\text{C}1^{4-}$  (Figure 1b and SI Figure S4b), substantiating the

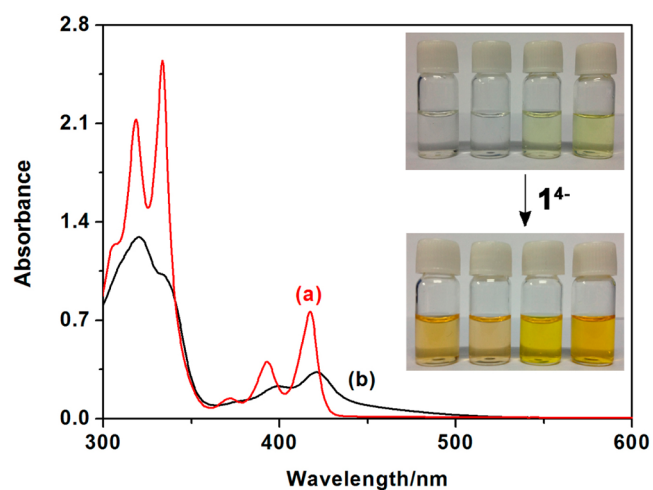


**Figure 1.** UV/vis absorption spectra of (a) the spectral sum of the individual components  $1^{4-}$  and  $\text{DMDAP}^{2+}$  and (b) complex  $\text{DMDAP}^{2+}\text{C}1^{4-}$  in water at 20 °C ( $[1^{4-}] = [\text{DMDAP}^{2+}] = 5.0 \times 10^{-5} \text{ M}$ ). Inset: visible color changes of  $\text{DP}^{2+}$ ,  $\text{BV}^{2+}$ ,  $\text{DMDAP}^{2+}$ , and  $\text{DBDAP}^{2+}$  (from left to right) in the absence and presence of  $1^{4-}$ .

significant CT interaction between the electron-donating naphthalenesulfonic moieties and the electron-accepting  $\text{DAP}^{2+}$  units. Similarly, in the case of  $\text{BV}^{2+}\text{C}1^{4-}$  and  $\text{DP}^{2+}\text{C}1^{4-}$ , the new CT absorbance bands centered at 448 nm and the shoulder peak around 480 nm were clearly observed upon addition of equimolar  $1^{4-}$  to  $\text{BV}^{2+}$  and  $\text{DP}^{2+}$  solution, respectively (Figures S5 and S6 in the Supporting Information).

It is noteworthy that the CT absorption strength in  $\text{DMDAP}^{2+}\text{C}1^{4-}$  and  $\text{DBDAP}^{2+}\text{C}1^{4-}$  is much stronger than the one in  $\text{BV}^{2+}\text{C}1^{4-}$  and  $\text{DP}^{2+}\text{C}1^{4-}$  at the same concentration. These phenomena should be ascribable to the larger  $\pi$ -aromatic coplanarity of  $\text{DAP}^{2+}$ , which would facilitate the electronic communication between the naphthalenesulfonic groups of  $1^{4-}$  and diazapyrenium conjugate of  $\text{DMDAP}^{2+}$  and  $\text{DBDAP}^{2+}$  in the ground state. In addition, the donor–acceptor interaction in these supramolecular complexes could also be readily distinguished by the characteristic color change of the solution. The dicationic substrates alone are colorless or pale yellow, but instantly turn to brilliant orange in the presence of macrocycle  $1^{4-}$  (inset photos in Figure 1). Furthermore, the electrochemical properties were investigated by the cyclic voltamme-

try. As seen in SI Figures S7–S9, the first reduction potentials of  $MV^{2+}$ ,  $DP^{2+}$ , and  $DMDAP^{2+}$  exhibit an obvious negative shift after adding 1 equiv of  $I^{4-}$ , suggesting that the guest molecules are stabilized by the water-soluble crown ether through the cooperative noncovalent interaction. In addition, it is found that the potential change of  $DMDAP^{2+}C1^{4-}$  (192 mV) is more pronounced than the ones of  $MV^{2+}C1^{4-}$  and  $DP^{2+}C1^{4-}$  (13 and 74 mV), which may be contributed to by the relatively higher binding affinity between  $DMDAP^{2+}$  and  $I^{4-}$ .

**$^1H$  NMR Titration.** Subsequently, the host–guest complexation between  $I^{4-}$  and four organic cations were further investigated by  $^1H$  NMR titration in  $D_2O$  at 25 °C, using acetone at 2.22 ppm as the internal standard. As shown in Figure 2, although some of the aromatic proton signals in

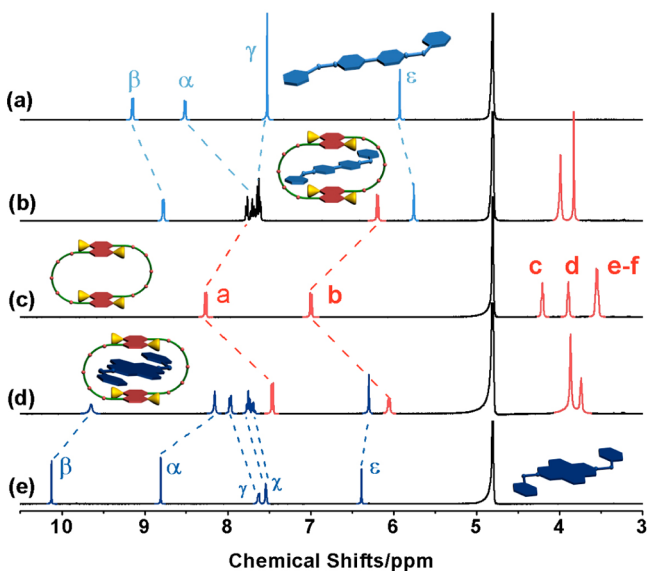


**Figure 2.** Partial  $^1H$  NMR spectra of (a)  $BV^{2+}$ , (b)  $BV^{2+}C1^{4-}$ , (c)  $I^{4-}$ , (d)  $DBDAP^{2+}C1^{4-}$ , and (e)  $DBDAP^{2+}$  in  $D_2O$  at 25 °C, respectively (400 MHz,  $[I^{4-}] = [BV^{2+}] = [DBDAP^{2+}] = 2.0 \times 10^{-3}$  M).

$BV^{2+}C1^{4-}$  are integrated into 7.58–7.80 ppm and thus cannot be accurately assigned (Figure 2b), the chemical shift changes ( $\Delta\delta$ ) of complexes  $BV^{2+}C1^{4-}$  and  $DBDAP^{2+}C1^{4-}$  still exhibit a similar tendency; that is, the aromatic protons ( $H_{\alpha}$  and  $H_{\beta}$ ) and the methylene sites of benzyl groups ( $H_{\epsilon}$ ) in  $BV^{2+}$  and  $DBDAP^{2+}$  undergo an obvious complex-induced upfield shift ( $\Delta\delta_{\beta,BV^{2+}C1^{4-}} = -0.37$  ppm,  $\Delta\delta_{\epsilon,BV^{2+}C1^{4-}} = -0.17$  ppm,  $\Delta\delta_{\beta,DBDAP^{2+}C1^{4-}} = -0.57$  ppm,  $\Delta\delta_{\alpha,DBDAP^{2+}C1^{4-}} = -0.65$  ppm, and  $\Delta\delta_{\epsilon,DBDAP^{2+}C1^{4-}} = -0.09$  ppm), whereas the phenyl protons in benzyl groups ( $H_{\gamma}$ ) of  $BV^{2+}$  and  $DBDAP^{2+}$  are split into multiplets and give a moderate downfield shift upon complexation ( $\Delta\delta_{\gamma,DBDAP^{2+}C1^{4-}} = 0.34$  ppm and  $\Delta\delta_{\chi,DBDAP^{2+}C1^{4-}} = 0.16$  and 0.22 ppm). Moreover, in addition to the peak pattern changes in the tetraethylene glycol linkers, there is also a remarkable upfield shift for the naphthyl protons ( $H_a$  and  $H_b$ ) of  $I^{4-}$  in these two complexes ( $\Delta\delta_{b,BV^{2+}C1^{4-}} = -0.80$  ppm,  $\Delta\delta_{a,DBDAP^{2+}C1^{4-}} = -0.81$  ppm, and  $\Delta\delta_{b,DBDAP^{2+}C1^{4-}} = -0.94$  ppm). These different variations in the  $\Delta\delta$  values of aromatic centers and benzyl units demonstrate that the aromatic centers of  $BV^{2+}$  and  $DBDAP^{2+}$  are trapped in the cavity of water-soluble crown ether  $I^{4-}$  by a combination of face-centered  $\pi$ -stacking with the naphthyl planes and C–H $\cdots$ O hydrogen-bonding interactions with the polyether side chains, while the pendant benzyl units of  $BV^{2+}$  and  $DBDAP^{2+}$  are located outside the crown ether ring.

Moreover, Job's plot was performed to explore the binding stoichiometry, in which the chemical shifts of  $H_{\epsilon}$  on  $DMDAP^{2+}$  and  $DBDAP^{2+}$  versus the molar ratio show an inflection point at 0.5, revealing a 1:1 complexation stoichiometry in  $DMDAP^{2+}C1$  and  $DBDAP^{2+}C1$  (Figures S10 and S11 in the Supporting Information). In addition, the formation of a 1:1 complex was further confirmed by electrospray ionization–mass spectrometry (ESI-MS). The  $m/z$  peaks at 645.5 and 1313.2 should be assigned to  $[(I^{4-} + BV^{2+})/2]^{-}$  and  $[I^{4-} + BV^{2+} + Na^{+}]^{-}$ , respectively, and the  $m/z$  peaks at 669.2 and 1340.3 should be assigned to  $[(I^{4-} + DBDAP^{2+})/2]^{-}$  and  $[I^{4-} + DBDAP^{2+} + H^{+}]^{-}$ , respectively (Figures S12 and S13 in the Supporting Information).

The  $^1H$  NMR spectra of  $DP^{2+}C1^{4-}$  and  $DMDAP^{2+}C1^{4-}$  are illustrated in Figure 3. Lacking benzyl groups, it can be seen

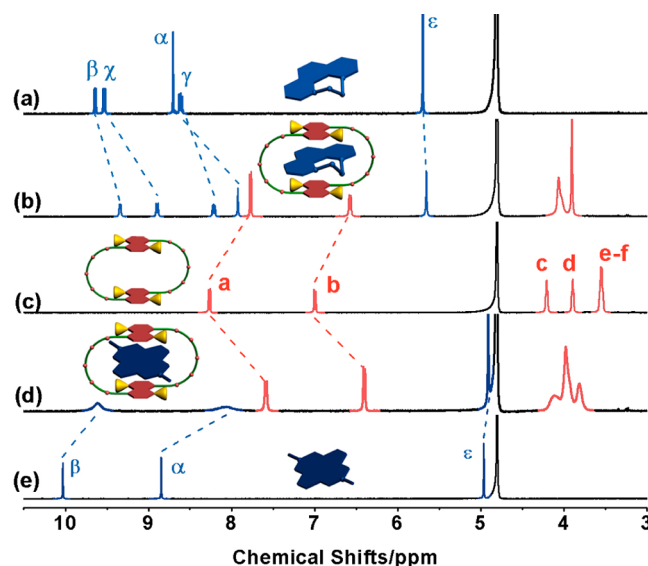


**Figure 3.** Partial  $^1H$  NMR spectra of (a)  $DP^{2+}$ , (b)  $DP^{2+}C1^{4-}$ , (c)  $I^{4-}$ , (d)  $DMDAP^{2+}C1^{4-}$ , and (e)  $DMDAP^{2+}$  in  $D_2O$  at 25 °C, respectively (400 MHz,  $[I^{4-}] = [DP^{2+}] = [DMDAP^{2+}] = 2.0 \times 10^{-3}$  M).

that all of the aromatic protons ( $H_{a-b}$ ,  $H_{\alpha-\beta}$ , and  $H_{\gamma-\chi}$ ), as well as the alkyl groups ( $H_{\epsilon}$ ) in these 1:1 host–guest mixtures, exhibit a significant upfield shift upon complexation. As shown in Figure 3a,b, the corresponding  $\Delta\delta$  values in  $H_{\alpha-\beta}$  in  $DP^{2+}C1^{4-}$  ( $\Delta\delta_{\alpha,DP^{2+}C1^{4-}} = -0.78$  ppm and  $\Delta\delta_{\beta,DP^{2+}C1^{4-}} = -0.30$  ppm) are much larger than the one in  $H_{\epsilon}$  ( $\Delta\delta_{\epsilon,DP^{2+}C1^{4-}} = -0.04$  ppm), mainly due to the ethylene spacer out of the  $\pi$ -aromatic plane of  $DP^{2+}$  that cannot make an intense interrelation with  $I^{4-}$ . Furthermore, in contrast to  $DP^{2+}C1^{4-}$ , the sizable upfield shifts in  $H_{\alpha-\beta}$  ( $\Delta\delta_{\alpha,DMDAP^{2+}C1^{4-}} = -0.80$  ppm and  $\Delta\delta_{\beta,DMDAP^{2+}C1^{4-}} = -0.42$  ppm) and  $H_{a-b}$  ( $\Delta\delta_{b,DMDAP^{2+}C1^{4-}} = -0.60$  ppm and  $\Delta\delta_{a,DMDAP^{2+}C1^{4-}} = -0.69$  ppm) of  $DMDAP^{2+}C1^{4-}$  are unanimously originated from the cooperative  $\pi$ -stacking arrangements that can induce a stronger shielding effect on these aromatic protons. Moreover, it is also found that the NMR signals of the diazapyrenium unit in  $DMDAP^{2+}C1^{4-}$  ( $H_{\alpha-\beta,DMDAP^{2+}C1^{4-}}$ ) are drastically broadened in the presence of  $I^{4-}$  (Figure 3d), which is distinctive from the ones in other complexes with a simple pattern of proton signals. These phenomena are mainly ascribable to a rigidified conformation upon association that forces the  $DMDAP^{2+}$  backbone to make a closer contact with the crown ether cavity  $I^{4-}$ , as recently exemplified by the incorporation of small-sized tetrasulfonated

1,5-dinaphtho-32-crown-8 with the relatively large-sized pyromellitic diimide and naphthalene diimide derivatives.<sup>29</sup> Moreover, it is found that the complexation of  $1^{4-}$  with  $\text{DMDAP}^{2+}$  exhibits a *slow exchange* equilibrium process, from which both the free and bound host molecules could be distinguished on the  $^1\text{H}$  NMR time scale (Figure S14 in the Supporting Information). For comparative purpose, the  $\Delta\delta$  values for all of the examined supramolecular complexes are summarized in SI Table S1. Similarly, the  $m/z$  peaks at 580.3 and 1161.2 in  $\text{DP}^{2+}\text{C}1^{4-}$  should be assigned to  $[(1^{4-} + \text{DP}^{2+})/2]^-$  and  $[1^{4-} + \text{DP}^{2+} + \text{H}^+]^-$ , respectively, and the  $m/z$  peaks at 593.3 and 1187.2 in  $\text{DMDAP}^{2+}\text{C}1^{4-}$  should be assigned to  $[(1^{4-} + \text{DMDAP}^{2+})/2]^-$  and  $[1^{4-} + \text{DMDAP}^{2+} + \text{H}^+]^-$ , respectively (Figures S15 and S16 in the Supporting Information).

Furthermore, the rotating-frame Overhauser effect spectroscopy (ROESY) experiments were performed to obtain the conformational changes upon host–guest complexation. As discerned from SI Figure S17, peaks A and A' are assigned to the nuclear Overhauser enhancement (NOE) correlations between  $H_{\alpha,\text{DMDAP}^{2+}}$  and  $H_{\beta,1^{4-}}$ , and peaks B–B' and C–C' are assigned to the NOE correlations of  $H_{\beta,\text{DMDAP}^{2+}}$  with the naphthyl rings ( $H_{\alpha,1^{4-}}$ ) and polyether chains ( $H_{\text{e-f},1^{4-}}$ ). Meanwhile, the NOE cross-peaks were also observed in  $\text{DBDAP}^{2+}$  with the naphthyl groups (peaks A–D and A'–D') and tetraethylene glycol chains (peaks E–F and E'–F') of  $1^{4-}$  (Figure S18 in the Supporting Information). Based on these conformational analyses, we can reasonably infer that the  $\text{DAP}^{2+}$  moiety is compactly surrounded by the cavity of  $1^{4-}$  to facilitate their mutual electrostatic attraction and  $\pi$ -stacking interaction in solution.

**Crystal Structures.** To gain more insight into the molecular binding behaviors in the solid state, two crystalline complexes of  $\text{DP}^{2+}\text{C}1^{4-}$  and  $\text{DMDAP}^{2+}\text{C}1^{4-}$  were initially prepared by the slow vapor diffusion method.<sup>40</sup> As shown in Figure 4, the [2]pseudorotaxanes of  $\text{DP}^{2+}\text{C}1^{4-}$  and

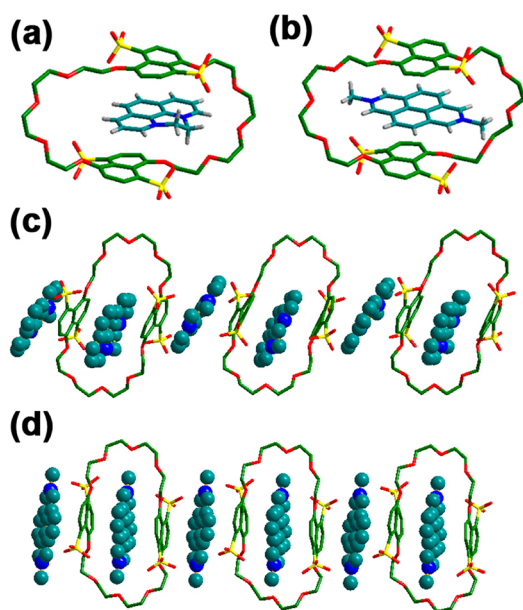


**Figure 4.** Crystal structures of [2]pseudorotaxanes (a)  $\text{DP}^{2+}\text{C}1^{4-}$  and (b)  $\text{DMDAP}^{2+}\text{C}1^{4-}$ , and packing representation of (c)  $\text{DP}^{2+}\text{C}1^{4-}$  and (d)  $\text{DMDAP}^{2+}\text{C}1^{4-}$ . Please note that the solvent molecules and partial hydrogen atoms are omitted for clarity.

$\text{DMDAP}^{2+}\text{C}1^{4-}$  consist of two types of guests; that is, one molecule is internally encapsulated in the cavity through the face-to-face  $\pi$ -stacking arrangements and  $\text{C}-\text{H}\cdots\text{O}$  hydrogen-bonding networks,<sup>41</sup> whereas the other one is externally bound to the sulfated sites of  $1^{4-}$  as counterion. Concretely, in the case of  $\text{DP}^{2+}\text{C}1^{4-}$ , the average interplanar distances between two naphthalene rings and phenanthroline plane are measured as 3.36 and 3.51 Å, respectively, accompanied by the intermolecular  $\text{C}-\text{H}\cdots\text{O}$  hydrogen-bonding networks of the phenanthroline plane with polyether chains and the distorted ethylene linker in  $\text{DP}^{2+}$  with sulfonated sites in  $1^{4-}$ .<sup>42</sup>

Superior to  $\text{DP}^{2+}\text{C}1^{4-}$ , it is found that in the crystallographic complex of  $\text{DMDAP}^{2+}\text{C}1^{4-}$ , the centroid–centroid distances between the  $\text{DMDAP}^{2+}$  plane and disulfonated naphthalene moiety are closer to 3.28 and 3.41 Å, respectively, which is more favorable for the effective aromatic  $\pi$ - $\pi$  interaction between donors and acceptors. In addition, there are more extensive intermolecular  $\text{C}-\text{H}\cdots\text{O}$  hydrogen-bonding interconnections between the glycol side chains of  $1^{4-}$  and  $\text{DMDAP}^{2+}$  to jointly fix the orientation in the interpenetrated structure of  $\text{DMDAP}^{2+}\text{C}1^{4-}$ .<sup>43</sup> Therefore, it is reasonable to suppose that the large disparities in these supramolecular architectures are generated from the host–guest complementarity (Figure S19 in the Supporting Information). That means,  $\text{DP}^{2+}$  with a low  $\pi$ -conjugated phenanthroline plane could not sufficiently occupy the crown ether cavity, whereas a compact packing complex is formed in  $\text{DMDAP}^{2+}\text{C}1^{4-}$  by a joint contribution of multiple noncovalent interactions to achieve the supramolecular positive cooperativity. More importantly, this preferable size/shape matching may be indicative of a higher affinity in the complexation of  $1^{4-}$  with  $\text{DMDAP}^{2+}$  in solution, which is further validated by their association constants and thermodynamic origins as described below.

**Thermodynamics.** The thermodynamic parameters in the supramolecular complexation of tetrasulfonated crown ether  $1^{4-}$  with four dicationic guests were quantitatively examined by means of isothermal titration calorimetry (ITC; Figures 5 and 6 and SI Figures S20–S23). In view of the extremely high stability in the complexes of  $1^{4-}$  with  $\text{DAP}^{2+}$ , a two-step competition titration was employed to indirectly obtain the corresponding equilibrium association constants ( $K_a$ ), in which  $\text{MV}^{2+}$  with a moderate  $K_a$  value of  $3.25 \times 10^5 \text{ M}^{-1}$  was used as the competitor. The thermodynamic parameters for  $1^{4-}$  with  $\text{MV}^{2+}$  in our previous work are also listed in Table 1. The typical competition ITC curves of  $\text{MV}^{2+}\text{C}1^{4-}$  upon the incremental addition of  $\text{DMDAP}^{2+}$  and  $\text{DBDAP}^{2+}$  are shown in Figure 6.

Comparatively, as shown in Table 1, the  $K_a$  values dramatically increase as the  $\pi$ -conjugation of aromatic moieties increases from the diquaternary salts of 4,4'-bipyridine and 1,10-phenanthroline, to 2,7-diazapyrene, with a maximum in the case of  $\text{DMDAP}^{2+}\text{C}1^{4-}$ . Benefiting from the suitable aromatic core of  $\text{DMDAP}^{2+}$  to fully occupy the crown ether cavity of  $1^{4-}$ , it is found that the  $K_a$  value of  $\text{DMDAP}^{2+}\text{C}1^{4-}$  can unprecedentedly reach  $1.12 \times 10^8 \text{ M}^{-1}$ , which overwhelms all of the reported thermodynamic stability in our previous work. In the previous results, the complexation between  $1^{4-}$  and  $\text{NDI}^{2+}$  gave the largest  $K_a$  value, and now, the complex of  $\text{DMDAP}^{2+}\text{C}1^{4-}$  successfully breaks this former record, ultimately resulting in 48 times higher enhancement in the

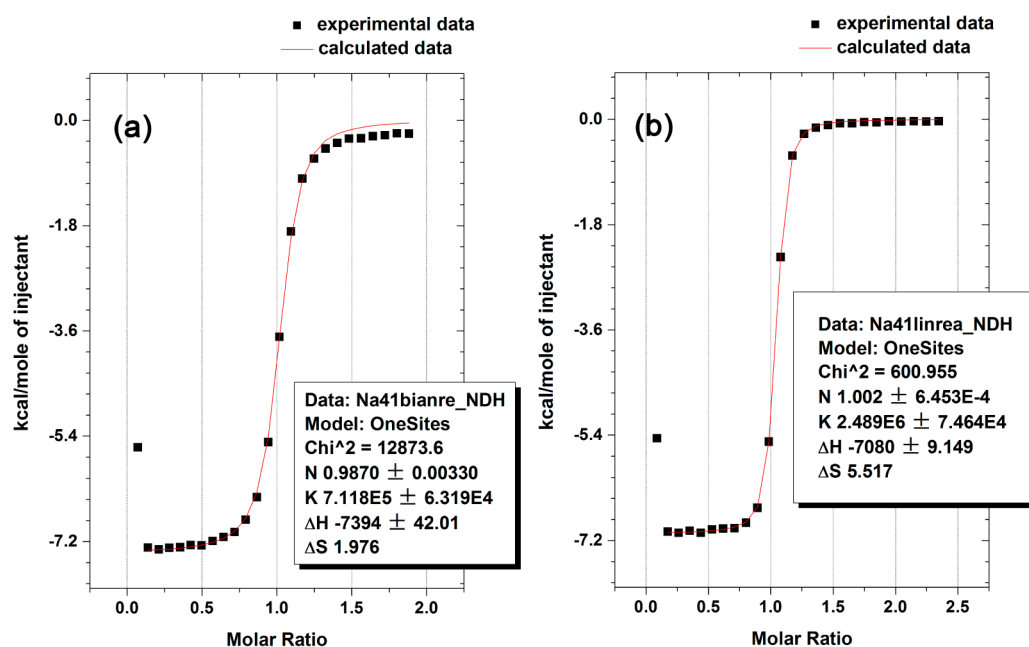


Figure 5. ITC experiments on complexation of (a)  $BV^{2+}C1^{4-}$  and (b)  $DP^{2+}C1^{4-}$  in neat water at 25 °C.

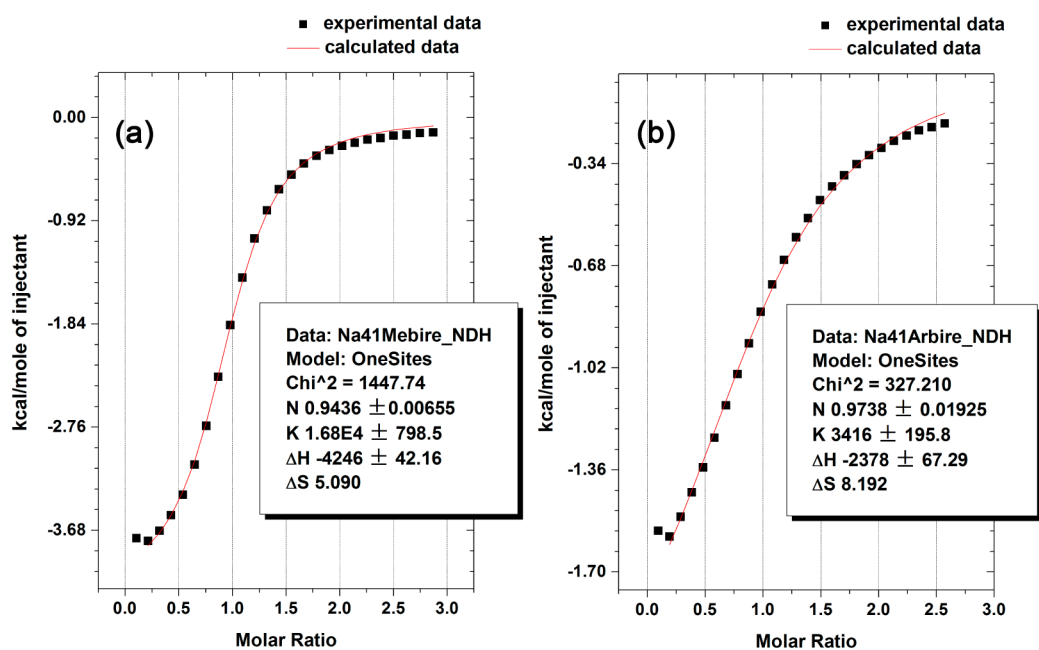


Figure 6. Competition ITC experiments on complexation of (a)  $DMDAP^{2+}$  and (b)  $DBDAP^{2+}$  with  $1^{4-}$  containing  $2.00 \times 10^{-2}$  M solution of  $MV^{2+}$  as competitor in neat water at 25 °C.

Table 1. Associate Constants ( $K_a/M^{-1}$ ), Standard Free Energy ( $\Delta G^\circ/(kJ \cdot mol^{-1})$ ), Enthalpy ( $\Delta H^\circ/(kJ \cdot mol^{-1})$ ), and Entropy Changes ( $T\Delta S^\circ/(kJ \cdot mol^{-1})$ ) for 1:1 Inclusion Complexation with  $1^{4-}$  in Water at 25 °C

guests	$K_a$	$-\Delta G^\circ$	$-\Delta H^\circ$	$T\Delta S^\circ$
$MV^{2+a}$	$(3.25 \pm 0.04) \times 10^5$	$31.46 \pm 0.03$	$30.13 \pm 0.24$	$1.33 \pm 0.21$
$BV^{2+b}$	$(7.12 \pm 0.01) \times 10^5$	$33.37 \pm 0.00$	$30.99 \pm 0.07$	$2.54 \pm 0.07$
$DP^{2+b}$	$(2.49 \pm 0.00) \times 10^6$	$36.47 \pm 0.00$	$29.80 \pm 0.06$	$6.84 \pm 0.06$
$DMDAP^{2+b}$	$(1.12 \pm 0.03) \times 10^8$	$45.89 \pm 0.06$	$47.84 \pm 0.12$	$-1.96 \pm 0.18$
$DBDAP^{2+b}$	$(2.25 \pm 0.03) \times 10^7$	$41.93 \pm 0.04$	$40.06 \pm 0.06$	$1.87 \pm 0.10$

<sup>a</sup>Reference 28. <sup>b</sup>This work.

stability and showing a good guest selectivity in this molecular recognition process ( $K_a^{\text{DMDAP}^{2+}\text{C1}^{4-}}/K_a^{\text{NDI}^{2+}\text{C1}^{4-}} = 48$ ).

Moreover, it should be noted that the benzyl groups in  $\text{BV}^{2+}$  and  $\text{DBDAP}^{2+}$  have different influence on the complex stability. In the complex of  $\text{BV}^{2+}\text{C1}^{4-}$ , the introduction of benzyl groups into the bispyridinium core can increase their  $K_a$  value to a certain extent ( $K_a^{\text{BV}^{2+}\text{C1}^{4-}}/K_a^{\text{MV}^{2+}\text{C1}^{4-}} = 2.2$ ), while this situation is distinctly changed in the case of  $\text{I}^{4-}$  with  $\text{DMDAP}^{2+}$  and  $\text{DBDAP}^{2+}$  ( $K_a^{\text{DMDAP}^{2+}\text{C1}^{4-}}/K_a^{\text{DBDAP}^{2+}\text{C1}^{4-}} = 5.0$ ). A quantitative investigation on the crystalline structures reveals that the closest interatomic distance between the positively charged nitrogen atom and the negatively charged sulfonated site in  $\text{DMDAP}^{2+}\text{C1}^{4-}$  ( $d_{\text{N3-O18}} = 2.91 \text{ \AA}$ ) is much shorter than the one in  $\text{MV}^{2+}\text{C1}^{4-}$  ( $d_{\text{N6-O8}} = 4.75 \text{ \AA}$ ), implying that there is still some free space in the loosely packed structure of  $\text{MV}^{2+}\text{C1}^{4-}$  (Figure S24 in the Supporting Information). Therefore, we can reasonably infer that the benzyl terminal groups around the relatively small-sized bispyridinium center in  $\text{BV}^{2+}$  could adjust its conformation to achieve the synergetic supramolecular cooperativity between phenyl and naphthyl rings. In contrast, the same groups in  $\text{DBDAP}^{2+}$  may act as a severe steric hindrance at the periphery of the large-sized  $\text{DAP}^{2+}$  center and thus bring the unfavorable factors in the formation of electrically interpenetrated complex with  $\text{I}^{4-}$ .

In addition, the binding abilities were further confirmed by UV/vis spectroscopic titration, in which the  $K_a$  values of  $\text{DMDAP}^{2+}\text{C1}^{4-}$  and  $\text{DBDAP}^{2+}\text{C1}^{4-}$  were calculated as  $4.6 \times 10^7 \text{ M}^{-1}$  and  $7.5 \times 10^6 \text{ M}^{-1}$ , respectively, by analyzing the sequential changes in absorption intensity ( $\Delta A$ ) of  $\text{I}^{4-}$  at varying concentrations of  $\text{DMDAP}^{2+}$  and  $\text{DBDAP}^{2+}$  by a nonlinear least-squares curve-fitting method. These reliable  $K_a$  values obtained by UV/vis titration are comparable to the ITC results (Figures S25 and S26 in the Supporting Information).

Thermodynamically, the binding process of  $\text{I}^{4-}$  with four dicationic guests is mostly controlled by the favorable enthalpic and entropic gains ( $-\Delta H^\circ = 29.80\text{--}47.84 \text{ kJ}\cdot\text{mol}^{-1}$  and  $T\Delta S^\circ = 1.33\text{--}6.84 \text{ kJ}\cdot\text{mol}^{-1}$ ), except the one in  $\text{DMDAP}^{2+}\text{C1}^{4-}$  with a slight entropic loss ( $T\Delta S^\circ_{\text{DMDAP}^{2+}\text{C1}^{4-}} = -1.96 \text{ kJ}\cdot\text{mol}^{-1}$ ). The dominant enthalpic gains definitely confirm that the mutual  $\pi$ -stacking interaction working at the aromatic components is the primary determinant to govern the molecular binding process. As shown in Table 1, despite the different molecular sizes and charge distributions of  $\text{BV}^{2+}$  and  $\text{DP}^{2+}$ , they have a quite similar  $\Delta H^\circ$  value ( $\Delta H^\circ_{\text{DP}^{2+}\text{C1}^{4-}} - \Delta H^\circ_{\text{BV}^{2+}\text{C1}^{4-}} = 1.19 \text{ kJ}\cdot\text{mol}^{-1}$ ). Conversely, as compared with  $\text{DBDAP}^{2+}\text{C1}^{4-}$ , the complexation in  $\text{DMDAP}^{2+}$  gives more favorable enthalpic gains ( $\Delta H^\circ_{\text{DBDAP}^{2+}\text{C1}^{4-}} - \Delta H^\circ_{\text{DMDAP}^{2+}\text{C1}^{4-}} = 7.78 \text{ kJ}\cdot\text{mol}^{-1}$ ), unequivocally corroborating the existence of significant donor–acceptor interaction in the complex of  $\text{DMDAP}^{2+}\text{C1}^{4-}$ .

Moreover, different from other dicationic substrates with a cyclic  $\pi$ -aromatic system, the flexible ethylene linker in the nonplanar structure of  $\text{DP}^{2+}$  could deter the positive charges from thoroughly delocalizing over the whole phenanthroline plane. As a result, the intensive positive charge on  $\text{DP}^{2+}$  facilitates a closer electrostatic contact between the oppositely charged sulfonated anions and quaternary ammonium cations, leading to the most favorable entropic gain in the complex of  $\text{DP}^{2+}\text{C1}^{4-}$ . This favorable entropic gain can substantially compensate the complex of  $\text{DP}^{2+}\text{C1}^{4-}$  for its inferiority in the enthalpic changes, and consequently, the standard free energy ( $\Delta G^\circ$ ) in  $\text{DP}^{2+}\text{C1}^{4-}$  is remarkably higher than the one in  $\text{BV}^{2+}\text{C1}^{4-}$  ( $\Delta G^\circ_{\text{BV}^{2+}\text{C1}^{4-}} - \Delta G^\circ_{\text{DP}^{2+}\text{C1}^{4-}} = 3.10 \text{ kJ}\cdot\text{mol}^{-1}$ ). On

the contrary, the larger coplanar  $\pi$ -aromatic unit of  $\text{DMDAP}^{2+}$  can dramatically reduce the charge density on the whole aromatic plane, which not only gives a stronger  $\pi$ -stacking interaction to form a tightly packed supramolecular complex with tetrasulfonated crown ether  $\text{I}^{4-}$  but also results in the large loss of conformational freedom during the host–guest binding process. Therefore, the high size-fit efficiency and conformational immobilization upon complexation are jointly responsible for the obvious entropic loss in the complex of  $\text{DMDAP}^{2+}\text{C1}^{4-}$ .

**Multicomponent Assembly in Aqueous Solution and the Solid State.** With the thermodynamic parameters and spectroscopic results in hand, we are able to construct a multicomponent system with  $\text{I}^{4-}$  and dicationic guests.<sup>44</sup> In this case, two groups of supramolecular complexes ( $\text{MV}^{2+}\text{C1}^{4-}$  and  $\text{DMDAP}^{2+}\text{C1}^{4-}$ ) with the strikingly different binding affinities were chosen to check the possibility in the formation of multicomponent architectures. As shown in Table 1, the  $K_a$  values of  $\text{MV}^{2+}\text{C1}^{4-}$  and  $\text{DMDAP}^{2+}\text{C1}^{4-}$  give an extremely higher selectivity ( $K_a^{\text{DMDAP}^{2+}\text{C1}^{4-}}/K_a^{\text{MV}^{2+}\text{C1}^{4-}} = 345$ ), which allows us to systematically monitor their host–guest competitive process using UV/vis and  $^1\text{H}$  NMR titration methods. As expected, the UV/vis spectra of  $\text{MV}^{2+}\text{C1}^{4-}$  in the presence of  $\text{DMDAP}^{2+}$  and  $\text{DBDAP}^{2+}$  are quite similar to the ones of  $\text{DMDAP}^{2+}\text{C1}^{4-}$  and  $\text{DBDAP}^{2+}\text{C1}^{4-}$ , indicating that  $\text{MV}^{2+}$  is expelled from the cavity of crown ether (SI Figure S27c,d and S27e,f).

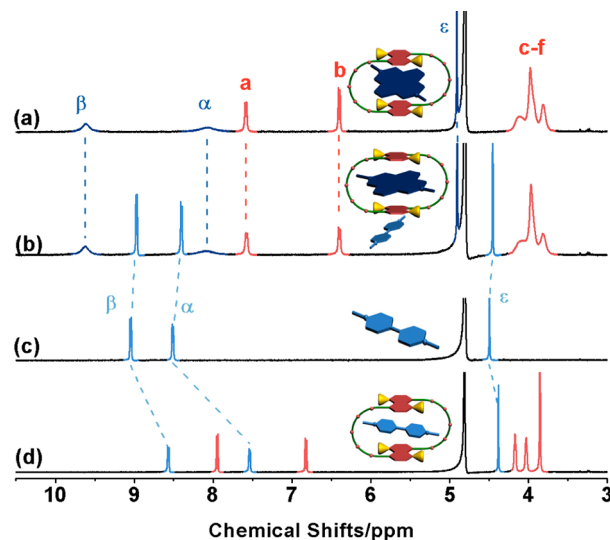


**Figure 7.** Partial  $^1\text{H}$  NMR spectra of (a)  $\text{DMDAP}^{2+}\text{C1}^{4-}$ , (b)  $\text{MV}^{2+}\text{C1}^{4-}$  upon addition of  $\text{DMDAP}^{2+}$ , (c)  $\text{MV}^{2+}$ , and (d)  $\text{MV}^{2+}\text{C1}^{4-}$  in  $\text{D}_2\text{O}$  at  $25^\circ\text{C}$ , respectively (400 MHz,  $[\text{I}^{4-}] = [\text{MV}^{2+}] = [\text{DMDAP}^{2+}] = 2.0 \times 10^{-3} \text{ M}$ ).

After adding 1 equiv of  $\text{DMDAP}^{2+}$ , the resonances of aromatic protons  $\text{H}_{\alpha-\beta, \text{MV}^{2+}\text{C1}^{4-}}$  at 7.54 and 8.58 ppm and nonaromatic protons  $\text{H}_{\epsilon, \text{MV}^{2+}\text{C1}^{4-}}$  at 4.38 ppm are almost completely restored at 8.41, 8.98, and 4.45 ppm, respectively (Figure 7b,d). As a consequence, the resulting complex of  $\text{MV}^{2+}\text{DMDAP}^{2+}\text{C1}^{4-}$  just resembles the simple superposition of  $\text{DMDAP}^{2+}\text{C1}^{4-}$  and free  $\text{MV}^{2+}$  (Figure 7a,c). Moreover, from the detailed  $^1\text{H}$  NMR titration experiments, it is found that the naphthyl protons of  $\text{I}^{4-}$  are first split into two peaks ( $\text{H}_{\text{a-a'}}$  and  $\text{H}_{\text{b-b'}}$ ) and then changed to one single resonance

peak at 6.32 and 7.50 ppm (Figure S28 in the Supporting Information). These phenomena jointly indicate that DMDAP<sup>2+</sup> gradually replaces MV<sup>2+</sup> to occupy the cavity of I<sup>4-</sup>. It should be noted that the reliable binding constant between MV<sup>2+</sup> and DMDAP<sup>2+</sup>·C1<sup>4-</sup> cannot be calculated by ITC or <sup>1</sup>H NMR titration in water, mainly due to the rather weak interaction of MV<sup>2+</sup> with the exterior surface of the crown ether ring. These results definitely demonstrate that the dominant supramolecular species in solution is DMDAP<sup>2+</sup>·C1<sup>4-</sup>, while the proportion of MV<sup>2+</sup>·C1<sup>4-</sup> is negligibly small in this

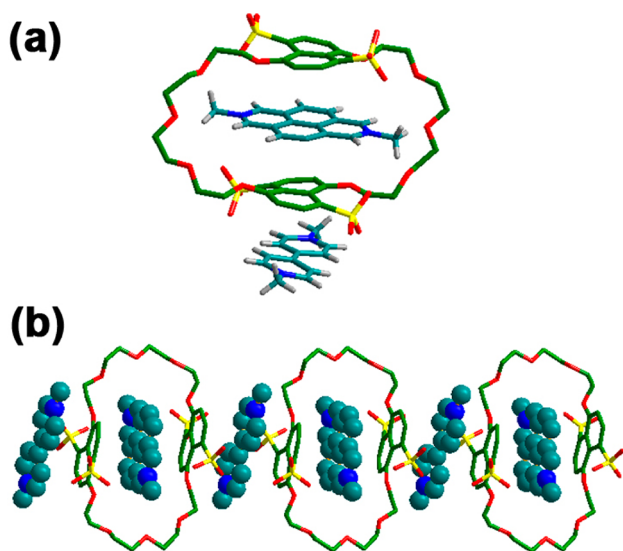


**Figure 8.** Crystal structures of (a) the repeating unit and (b) the packing representation of ternary complex MV<sup>2+</sup>·DMDAP<sup>2+</sup>·C1<sup>4-</sup>. Please note that the solvent molecules and partial hydrogen atoms are omitted for clarity.

ternary system of MV<sup>2+</sup>·DMDAP<sup>2+</sup>·C1<sup>4-</sup>. The  $\Delta\delta$  values for this multicomponent assembly are summarized in SI Table S2.

To provide further evidence to support this specific binding process, the crystal structure of MV<sup>2+</sup>·DMDAP<sup>2+</sup>·C1<sup>4-</sup> was also obtained by the slow vapor diffusion of the equimolar mixture containing I<sup>4-</sup>, MV<sup>2+</sup>, and DMDAP<sup>2+</sup> (Figure 8). Interestingly, it can be found that the repeating unit of this ternary complex is comprised of one host and two different guests, where one DMDAP<sup>2+</sup> is steadily included in the crown ether cavity to form [2]pseudorotaxane, and another MV<sup>2+</sup> is located in the crystal lattice as counterion to synergistically stabilize the topological structures. The average interplanar distances between two naphthalene moieties and the external face of DMDAP<sup>2+</sup> are measured as 3.30 and 3.38 Å, respectively, which are very close to the ones in the complex of DMDAP<sup>2+</sup>·C1<sup>4-</sup> (Figure 4b,d). The similar interplanar separation and the effective hydrogen bonds<sup>45</sup> in MV<sup>2+</sup>·DMDAP<sup>2+</sup>·C1<sup>4-</sup> imply that the introduction of MV<sup>2+</sup> into the ternary system could not make any tremendous impact on the intermolecular geometry between DMDAP<sup>2+</sup> and I<sup>4-</sup>. Therefore, with combination of the aforementioned NMR analyses with the crystallographic structures, it is convincingly proven that once MV<sup>2+</sup>·C1<sup>4-</sup> encounters DMDAP<sup>2+</sup>, they can spontaneously approach a selective binding process in both aqueous solution and the solid state. Since there is not enough space in I<sup>4-</sup> to simultaneously accommodate two kinds of guest molecules, MV<sup>2+</sup> with a rather lower supramolecular affinity is forced to release from the

crown ether cavity and then interlace with the [2]-pseudorotaxane structure of DMDAP<sup>2+</sup>·C1<sup>4-</sup> in the solid state. The different binding behaviors of MV<sup>2+</sup> and DMDAP<sup>2+</sup> with I<sup>4-</sup> in solution and the solid state reveal that the crystallization process can cross the barrier of weak interaction between MV<sup>2+</sup> and complex DMDAP<sup>2+</sup>·C1<sup>4-</sup> in water and thus lead to a topologically polymeric [2]-pseudorotaxane in the solid state.

## CONCLUSION

In summary, the inclusion complexation behaviors of the tetrasulfonato crown ether I<sup>4-</sup> with BV<sup>2+</sup>, DP<sup>2+</sup>, DMDAP<sup>2+</sup>, and DBDAP<sup>2+</sup> are systematically investigated, exhibiting a more enhanced  $K_a$  value up to 10<sup>8</sup> M<sup>-1</sup> order of magnitude in complex DMDAP<sup>2+</sup>·C1<sup>4-</sup>. Different from our previous results, the electrostatic attraction is replaced by the  $\pi$ -stacking interaction as the most important driving force to preorganize the host–guest superstructures. These obtained results can greatly overcome the obstacles of binding affinity in the flexible and large-sized crown ether and then lead to a multicomponent assembly of MV<sup>2+</sup>·DMDAP<sup>2+</sup>·C1<sup>4-</sup> involving two different guest molecules in the solid state. The  $K_a$  gradient and the corresponding thermodynamic properties of large-sized crown ether I<sup>4-</sup> are now preliminarily implemented in our systematic work, which can largely improve our understanding of the structural organization in the crown ether molecular recognition process. Moreover, the thermodynamically favorable complexation in this work further emphasizes the importance of host–guest complementarity in the charge distribution and geometric configuration, by which other primary noncovalent driving forces, such as  $\pi$ -stacking, electrostatic attraction, and hydrogen-bonding interactions, can be continuously stimulated to propagate the formation of highly ordered nanoarchitectures. We also envisage that by elaborately designing the “smart” guests with the adaptive capacity to macrocyclic hosts, one can create a library of sophisticated and advanced crown ether based molecular machines in water.

## EXPERIMENTAL SECTION

**General Method.** All chemicals were commercially available unless noted otherwise. Host compound I<sup>4-</sup> was prepared by our previous method and used with its sodium salts.<sup>28</sup> Guest molecules MV<sup>2+</sup>, BV<sup>2+</sup>, DP<sup>2+</sup>, and DBDAP<sup>2+</sup> were synthesized according to the reported literature<sup>46–48</sup> and used with their bromine salts. NMR data were recorded on a 400 MHz spectrometer. All chemical shifts were referenced to the internal acetone signal at 2.22 ppm.<sup>49</sup> Absorption spectra were recorded on a UV/vis spectrometer.

The crystals of DP<sup>2+</sup>·C1<sup>4-</sup>, DMDAP<sup>2+</sup>·C1<sup>4-</sup>, and MV<sup>2+</sup>·DMDAP<sup>2+</sup>·C1<sup>4-</sup> were obtained by the slow vapor diffusion of acetone into aqueous solution of the corresponding 1:1 host–guest complexes. The resultant solution was kept at room temperature for about 10 days, and then the crystalline complexes could be collected for X-ray crystallographic analysis. All of the X-ray intensity data were obtained on a rotating anode diffractometer equipped with a CCD Area Detector System, using monochromated Mo K $\alpha$  ( $\lambda = 0.71073$  Å) radiation at  $T = 113(2)$  K. CCDC Nos. 957254, 957255, and 957342 contain the supplementary crystallographic data for complexes DP<sup>2+</sup>·C1<sup>4-</sup>, DMDAP<sup>2+</sup>·C1<sup>4-</sup>, and MV<sup>2+</sup>·DMDAP<sup>2+</sup>·C1<sup>4-</sup> in this work, respectively. These data can be

obtained free of charge from the Cambridge Crystallographic Data Centre via [www.ccdc.cam.ac.uk/data\\_request/cif](http://www.ccdc.cam.ac.uk/data_request/cif).

A thermostatted and fully computer-operated isothermal calorimetry instrument was used for all of the microcalorimetric experiments. The ITC experiments were performed at 25 °C in aqueous solution, giving the association constants ( $K_a$ ) and the thermodynamic parameters ( $\Delta H$  and  $\Delta S$ ) upon complexation. In each run, a solution of guest in a 0.250 mL syringe was sequentially injected with stirring at 300 rpm into a solution of host in the sample cell (1.4227 mL volume). A control experiment to determine the heat of dilution was carried out for each run by performing the same number of injections with the same concentration of guest compound as used in the titration experiments into a same solution in the absence of host compound or competitive complex. The dilution enthalpies determined in control experiments were subtracted from the enthalpies measured in the titration experiments to obtain the net reaction heat. All thermodynamic parameters reported in this work were obtained by using the “one set of binding sites” model. Two titration experiments were independently performed to give the averaged values with reasonable errors.

In our system, a multistep competition method was employed in the ITC experiments with  $MV^{2+}$  as the competitor, because the association constants of the complexation between  $1^{4+}$  with  $DMDAP^{2+}$  and  $DBDAP^{2+}$  are extremely large ( $>10^6 M^{-1}$ ). Then, the  $K_a$  value of complex and the total reaction enthalpy ( $\Delta H^\circ$ ) could be calculated according to the following equations:

$$K_a = [\text{competitor}]K_{\text{exp}}K_{\text{competitor}}$$

$$\Delta H^\circ = \Delta H^\circ_{\text{exp}} + \Delta H^\circ_{\text{competitor}}$$

where  $K_{\text{exp}}$  and  $\Delta H^\circ_{\text{exp}}$  are the measured association constant and reaction enthalpy of  $1^{4+}$  with  $DMDAP^{2+}$  or  $DBDAP^{2+}$  in the presence of  $MV^{2+}$ , respectively, and  $K_{\text{competitor}}$  and  $\Delta H^\circ_{\text{competitor}}$  are the known association constant and reaction enthalpy between  $1^{4+}$  and  $MV^{2+}$ , respectively.

**Synthesis of 2,7-Dimethyldiazapyrenium bromine salt ( $DMDAP \cdot Br_2$ ).** Briefly, the  $PF_6^-$  counterion of 2,7-dimethyldiazapyrenium salt<sup>50</sup> was converted to  $Br^-$  ion through a standard counterion exchange using tetraethylammonium bromide in  $CH_3CN$ .  $^1H$  NMR (400 MHz,  $D_2O$ , ppm):  $\delta$  9.91 (s, 4H), 8.72 (s, 4H), 4.84 (s, 6H).  $^{13}C$  NMR (100 MHz,  $D_2O$ , ppm):  $\delta$  141.9, 129.9, 129.5, 126.8, 50.0. MALDI-MS.  $m/z$  calcd for  $C_{16}H_{14}Br_2N_2 [M - 2Br]^{2+}$ : 117.0578. Found: 117.0578.  $[M - H - 2Br]^{+}$ : 233.1071. Found: 233.1079.

## ■ ASSOCIATED CONTENT

### ■ Supporting Information

Figures showing characterization data of  $DMDAP \cdot Br_2$ , X-ray crystallographic data in CIF format, UV/vis and  $^1H$  NMR titration experiments, UV/vis absorption, 2D NMR, and ESI-MS spectra, cyclic voltammograms, Job's plots, molecular sizes obtained from crystal structures, calorimetric titration curves, and interatomic distances and tables listing chemical shift changes. This material is available free of charge via the Internet at <http://pubs.acs.org>.

## ■ AUTHOR INFORMATION

### Corresponding Author

\*E-mail: [yuliu@nankai.edu.cn](mailto:yuliu@nankai.edu.cn).

## Notes

The authors declare no competing financial interest.

## ■ ACKNOWLEDGMENTS

This work was financially supported by the 973 Program (Grant 2011CB932502) and NNSFC (Grant Nos. 20932004, 91227107, and 21102075).

## ■ REFERENCES

- (1) Schneider, H. J.; Yatsimirsky, A. K. Selectivity in Supramolecular Host–Guest Complexes. *Chem. Soc. Rev.* **2008**, *37*, 263–277.
- (2) Qu, D. H.; Tian, H. Novel and Efficient Templates for Assembly of Rotaxanes and Catenanes. *Chem. Sci.* **2011**, *2*, 1011–1015.
- (3) Ariga, K.; Ito, H.; Hill, J. P.; Tsukube, H. Molecular Recognition: From Solution Science to Nano/materials Technology. *Chem. Soc. Rev.* **2012**, *41*, 5800–5835.
- (4) Yilmaz, M. D.; Huskens, J. Orthogonal Supramolecular Interaction Motifs for Functional Monolayer Architectures. *Soft Matter* **2012**, *8*, 11768–11780.
- (5) Wang, M.-X. Nitrogen and Oxygen Bridged Calixaromatics: Synthesis, Structure, Functionalization, and Molecular Recognition. *Acc. Chem. Res.* **2012**, *45*, 182–195.
- (6) Ghosh, I.; Nau, W. M. The Strategic Use of Supramolecular pKa Shifts to Enhance the Bioavailability of Drugs. *Adv. Drug Delivery Rev.* **2012**, *64*, 764–783.
- (7) Gramage-Doria, R.; Armspach, D.; Matt, D. Metallated Cavitands (Calixarenes, Resorcinarenes, Cyclodextrins) with Internal Coordination Sites. *Coord. Chem. Rev.* **2013**, *257*, 776–816.
- (8) Gokel, G. W.; Leevy, W. M.; Weber, M. E. Crown Ethers: Sensors for Ions and Molecular Scaffolds for Materials and Biological Models. *Chem. Rev.* **2004**, *104*, 2723–2750.
- (9) Kralj, M.; Tušek-Božić, L.; Frkanec, L. Biomedical Potentials of Crown Ethers: Prospective Antitumor Agents. *ChemMedChem* **2008**, *3*, 1478–1492.
- (10) Zheng, B.; Wang, F.; Dong, S.; Huang, F. Supramolecular Polymers Constructed by Crown Ether-Based Molecular Recognition. *Chem. Soc. Rev.* **2012**, *41*, 1621–1636.
- (11) Liu, Y.; Chen, Y. Cooperative Binding and Multiple Recognition by Bridged Bis( $\beta$ -Cyclodextrin)s with Functional Linkers. *Acc. Chem. Res.* **2006**, *39*, 681–691.
- (12) Harada, A.; Hashidzume, A.; Yamaguchi, H.; Takashima, Y. Polymeric Rotaxanes. *Chem. Rev.* **2009**, *109*, 5974–6023.
- (13) Ortiz Mellet, C.; García Fernández, J. M.; Benito, J. M. Cyclodextrin-Based Gene Delivery Systems. *Chem. Soc. Rev.* **2011**, *40*, 1586–1608.
- (14) Dong, Z.; Luo, Q.; Liu, J. Artificial Enzymes Based on Supramolecular Scaffolds. *Chem. Soc. Rev.* **2012**, *41*, 7890–7908.
- (15) Leray, I.; Valeur, B. Calixarene-based Fluorescent Molecular Sensors for Toxic Metals. *Eur. J. Inorg. Chem.* **2009**, 3525–3535.
- (16) Creaven, B. S.; Donlon, D. F.; McGinley, J. Coordination Chemistry of Calix[4]arene Derivatives with Lower Rim Functionalisation and Their Applications. *Coord. Chem. Rev.* **2009**, *253*, 893–962.
- (17) Guo, D.-S.; Liu, Y. Calixarene-Based Supramolecular Polymerization in Solution. *Chem. Soc. Rev.* **2012**, *41*, 5907–5921.
- (18) Lee, J. W.; Samal, S.; Selvapalam, N.; Kim, H. J.; Kim, K. Cucurbituril Homologues and Derivatives: New Opportunities in Supramolecular Chemistry. *Acc. Chem. Res.* **2003**, *36*, 621–630.
- (19) Lagona, J.; Mukhopadhyay, P.; Chakrabarti, S.; Isaacs, L. The Cucurbit[n]uril Family. *Angew. Chem., Int. Ed.* **2005**, *44*, 4844–4870.
- (20) Masson, E.; Ling, X.; Joseph, R.; Kyeremeh-Mensah, L.; Lu, X. Cucurbituril Chemistry: A Tale of Supramolecular Success. *RSC Adv.* **2012**, *2*, 1213–1247.
- (21) Lü, J.; Lin, J. X.; Cao, M. N.; Cao, R. Cucurbituril: A Promising Organic Building Block for the Design of Coordination Compounds and Beyond. *Coord. Chem. Rev.* **2013**, *257*, 1334–1356.
- (22) Zhang, B.; Breslow, R. Enthalpic Domination of the Chelate Effect in Cyclodextrin Dimers. *J. Am. Chem. Soc.* **1993**, *115*, 9353–9354.

(23) Kano, K.; Nishiyabu, R.; Asada, T.; Kuroda, Y. Static and Dynamic Behavior of 2:1 Inclusion Complexes of Cyclodextrins and Charged Porphyrins in Aqueous Organic Media. *J. Am. Chem. Soc.* **2002**, *124*, 9937–9944.

(24) Jeon, W. S.; Moon, K.; Park, S. H.; Chun, H.; Ko, Y. H.; Lee, J. Y.; Lee, E. S.; Samal, S.; Selvapalam, N.; Rekharsky, M. V.; et al. Complexation of Ferrocene Derivatives by the Cucurbit[7]uril Host: A Comparative Study of the Cucurbituril and Cyclodextrin Host Families. *J. Am. Chem. Soc.* **2005**, *127*, 12984–12989.

(25) Rekharsky, M. V.; Mori, T.; Yang, C.; Ko, Y. H.; Selvapalam, N.; Kim, H.; Sobransingh, D.; Kaifer, A. E.; Liu, S.; Isaacs, L.; et al. A Synthetic Host–Guest System Achieves Avidin–Biotin Affinity by Overcoming Enthalpy–Entropy Compensation. *Proc. Natl. Acad. Sci. U. S. A.* **2007**, *104*, 20737–20742.

(26) Oshovsky, G. V.; Reinhoudt, D. N.; Verboom, W. Supramolecular Chemistry in Water. *Angew. Chem., Int. Ed.* **2007**, *46*, 2366–2393.

(27) Chen, L.; Zhang, Y.-M.; Liu, Y. Molecular Binding Behaviors between Tetrasulfonated Bis(*m*-phenylene)-26-crown-8 and Bispyridinium Guests in Aqueous Solution. *J. Phys. Chem. B* **2012**, *116*, 9500–9506.

(28) Chen, L.; Zhang, H.-Y.; Liu, Y. High Affinity Crown Ether Complexes in Water: Thermodynamic Analysis, Evidence of Crystallography and Binding of NAD<sup>+</sup>. *J. Org. Chem.* **2012**, *77*, 9766–9773.

(29) Chen, L.; Zhang, Y.-M.; Wang, L.-H.; Liu, Y. Molecular Binding Behaviors of Pyromellitic and Naphthalene Diimide Derivatives by Tetrasulfonated 1,5-Dinaphtho-(3*n*+8)-crown-*n* (*n* = 8, 10) in Aqueous Solution. *J. Org. Chem.* **2013**, *78*, 5357–5363.

(30) Lestini, E.; Nikitin, K.; Müller-Bunz, H.; Fitzmaurice, D. Introducing Negative Charges into Bis-*p*-phenylene Crown Ethers: A Study of Bipyridinium-Based [2]Pseudorotaxanes and [2]Rotaxanes. *Chem.—Eur. J.* **2008**, *14*, 1095–1106.

(31) Hoffart, D. J.; Tiburcio, J.; de la Torre, A.; Knight, L. K.; Loeb, S. J. Cooperative Ion–Ion Interactions in the Formation of Interpenetrated Molecules. *Angew. Chem., Int. Ed.* **2008**, *47*, 97–101.

(32) Nandhikonda, P.; Begaye, M. P.; Heagy, M. D. Highly water-soluble, OFF-ON, dual fluorescent probes for sodium and potassium ions. *Tetrahedron Lett.* **2009**, *50*, 2459–2461.

(33) Ji, X.; Zhang, M.; Yan, X.; Li, J.; Huang, F. Synthesis of a Water-Soluble Bis(*m*-phenylene)-32-crown-10-Based Cryptand and Its pH-Responsive Binding to a Quinazolinone Derivative. *Chem. Commun. (Cambridge, U. K.)* **2013**, *49*, 1178–1180.

(34) Ballardini, R.; Balzani, V.; Credi, A.; Gandolfi, M. T.; Langford, S. J.; Menzer, S.; Prodi, L.; Stoddart, J. F.; Venturi, M.; Williams, D. J. Simple Molecular Machines: Chemically Driven Unthreading and Rethreading of a [2]Pseudorotaxane. *Angew. Chem., Int. Ed.* **1996**, *35*, 978–981.

(35) Credi, A.; Balzani, V.; Langford, S. J.; Stoddart, J. F. Logic Operations at the Molecular Level. An XOR Gate Based on a Molecular Machine. *J. Am. Chem. Soc.* **1997**, *119*, 2679–2681.

(36) Ashton, P. R.; Ballardini, R.; Balzani, V.; Constable, E. C.; Credi, A.; Kocian, O.; Langford, S. J.; Preece, J. A.; Prodi, L.; Schofield, E. R.; et al. Ru<sup>II</sup>-Polypyridine Complexes Covalently Linked to Electron Acceptors as Wires for Light-Driven Pseudorotaxane-type Molecular Machines. *Chem.—Eur. J.* **1998**, *4*, 2413–2422.

(37) Sindelar, V.; Cejas, M. A.; Raymo, F. M.; Kaifer, A. E. Tight Inclusion Complexation of 2,7-Dimethyldiazapyrenium in Cucurbit[7]uril. *New J. Chem.* **2005**, *29*, 280–282.

(38) Sindelar, V.; Cejas, M. A.; Raymo, F. M.; Chen, W.; Parker, S. E.; Kaifer, A. E. Supramolecular Assembly of 2,7-Dimethyldiazapyrenium and Cucurbit[8]uril: A New Fluorescent Host for Detection of Catechol and Dopamine. *Chem.—Eur. J.* **2005**, *11*, 7054–7059.

(39) Ballardini, R.; Balzani, V.; Di Fabio, A.; Gandolfi, M. T.; Becher, J.; Lau, J.; Nielsen, M. B.; Stoddart, J. F. Macrocycles, Pseudorotaxanes and Catenanes Containing Apyrrolo-tetrathiafulvalene Unit: Absorption Spectra, Luminescence Properties and Redox Behavior. *New J. Chem.* **2001**, *25*, 293–298.

(40) Crystal data for DP<sup>2+</sup>C1<sup>4-</sup>: C<sub>64</sub>H<sub>90</sub>N<sub>4</sub>O<sub>34</sub>S<sub>4</sub>; *M* = 1587.64; orthorhombic; space group *Pna2*<sub>1</sub>; *a* = 31.150(6), *b* = 16.287(3), and *c* = 14.681(3) Å; α = 90°, β = 90°, and γ = 90°; *V* = 7448(3) Å<sup>3</sup>; *F*(000) = 3352; *Z* = 4; *D*<sub>c</sub> = 1.416 g·cm<sup>-3</sup>; μ = 0.220 mm<sup>-1</sup>; approx crystal dimens, 0.20 × 0.18 × 0.12 mm<sup>3</sup>; θ range = 1.31–25.02°; 46380 measd reflcs, of which 12642 (*R*<sub>int</sub> = 0.0486) were unique; final *R* indices [*I* > 2σ(*I*)], *R*<sub>1</sub> = 0.0697 and *wR*<sub>2</sub> = 0.1952; *R* indices (all data): *R*<sub>1</sub> = 0.0742 and *wR*<sub>2</sub> = 0.2011; goodness of fit on *F*<sup>2</sup> = 1.080. Crystal data for DMDAP<sup>2+</sup>C1<sup>4-</sup>: C<sub>68</sub>H<sub>84.50</sub>N<sub>4</sub>O<sub>30.25</sub>S<sub>4</sub>; *M* = 1570.14; triclinic; space group *P* $\bar{1}$ ; *a* = 8.3143(17), *b* = 14.653(3), and *c* = 30.316(6) Å; α = 77.39(3)°, β = 89.28(3)°, and γ = 87.12(3)°; *V* = 3599.8(13) Å<sup>3</sup>; *F*(000) = 1653; *Z* = 2; *D*<sub>c</sub> = 1.449 g·cm<sup>-3</sup>; μ = 0.224 mm<sup>-1</sup>; approx crystal dimens, 0.24 × 0.22 × 0.18 mm<sup>3</sup>; θ range = 1.71–25.02°; 26328 measd reflcs, of which 12421 (*R*<sub>int</sub> = 0.0573) were unique; final *R* indices [*I* > 2σ(*I*)], *R*<sub>1</sub> = 0.0796 and *wR*<sub>2</sub> = 0.2219; *R* indices (all data), *R*<sub>1</sub> = 0.0979 and *wR*<sub>2</sub> = 0.2370; goodness of fit on *F*<sup>2</sup> = 1.055.

(41) The valid hydrogen bonds in this work are defined as the ones with H⋯O distance less than 2.8 Å and C–H⋯O angle greater than 120°.

(42) The C–H⋯O hydrogen-bonding parameters [H⋯O distance (Å), C–H⋯O angle (deg), and C⋯O distance (Å)] in complex DP<sup>2+</sup>C1<sup>4-</sup> are shown as follows: for C37–H⋯O20, 2.32 Å, 165.9°, and 3.25 Å; for C49–H⋯O16, 2.51 Å, 125.5°, and 3.19 Å.

(43) The C–H⋯O hydrogen-bonding parameters [H⋯O distance (Å), C–H⋯O angle (deg), and C⋯O distance (Å)] in complex DMDAP<sup>2+</sup>C1<sup>4-</sup> are shown as follows: for C68–H⋯O3, 2.56 Å, 154.8°, and 3.47 Å; for C67–H⋯O8, 2.61 Å, 160.9°, and 3.55 Å; for C53–H⋯O8, 2.77 Å, 151.0°, and 3.53 Å; for C60–H⋯O20, 2.60 Å, 130.6°, and 3.32 Å; for C67–H⋯O11, 2.73 Å, 126.9°, and 3.41 Å.

(44) Crystal data for MV<sup>2+</sup>·DMDAP<sup>2+</sup>C1<sup>4-</sup>: C<sub>64</sub>H<sub>68</sub>N<sub>4</sub>O<sub>37.63</sub>S<sub>4</sub>; *M* = 1623.46; monoclinic; space group *P2*<sub>1</sub>; *a* = 14.115(12), *b* = 18.546(16), and *c* = 28.97(3) Å; α = 90°, β = 102.032(9)°, and γ = 90°; *V* = 7417(12) Å<sup>3</sup>; *F*(000) = 3380; *Z* = 4; *D*<sub>c</sub> = 1.454 g·cm<sup>-3</sup>; μ = 0.227 mm<sup>-1</sup>; approx crystal dimens, 0.30 × 0.28 × 0.24 mm<sup>3</sup>; θ range = 1.44–26.00°; 57328 measd reflcs, of which 27727 (*R*<sub>int</sub> = 0.0995) were unique; final *R* indices [*I* > 2σ(*I*)], *R*<sub>1</sub> = 0.0920 and *wR*<sub>2</sub> = 0.2105; *R* indices (all data), *R*<sub>1</sub> = 0.1432 and *wR*<sub>2</sub> = 0.2501; goodness of fit on *F*<sup>2</sup> = 0.917.

(45) The C–H⋯O hydrogen-bonding parameters [H⋯O distance (Å), C–H⋯O angle (deg), and C⋯O distance (Å)] in complex MV<sup>2+</sup>·DMDAP<sup>2+</sup>C1<sup>4-</sup> are shown as follows: for C87–H⋯O15, 2.54 Å, 139.6°, and 3.35 Å; for C88–H⋯O20, 2.64 Å, 167.4°, and 3.60 Å; for C88–H⋯O10, 2.57 Å, 136.3°, and 3.35 Å.

(46) Albrecht, M.; Yulikov, M.; Kohn, T.; Jeschke, G.; Adams, J.; Schmidt, A. Pyridinium Salts and Ylides as Partial Structures of Photoresponsive Merrifield Resins. *J. Mater. Chem.* **2010**, *20*, 3025–3034.

(47) Xiao, Y.; Chu, L.; Sanakis, Y.; Liu, P. Revisiting the IspH Catalytic System in the Deoxyxylulose Phosphate Pathway: Achieving High Activity. *J. Am. Chem. Soc.* **2009**, *131*, 9931–9933.

(48) Cejas, M. A.; Raymo, F. M. Fluorescent Diazapyrenium Films and Their Response to Dopamine. *Langmuir* **2005**, *21*, 5795–5802.

(49) Gottlieb, H. E.; Kotlyar, V.; Nudelman, A. NMR Chemical Shifts of Common Laboratory Solvents as Trace Impurities. *J. Org. Chem.* **1997**, *62*, 7512–7515.

(50) Ashton, P. R.; Langford, S. J.; Spencer, N.; Stoddart, J. F.; White, A. J. P.; Williams, D. J. The Self-Assembly of a Complex with a [3]Pseudorotaxane Superstructure. *Chem. Commun. (Cambridge, U. K.)* **1996**, 1387–1388.